Hybrid Investigation on the Hydraulic Performance of a New Trapezoidal Fishway

Daniel Bung
University of Applied Sciences FH Aachen, bung@fh-aachen.de

Daniel Valero
FH Aachen, valero@fh-aachen.de

G. Hermens
Ingenieurbüro Floecksmühle GmbH Aachen, gereon.hermens@floecksmuehle-fwt.de

Recommended Citation

Bung, Daniel (2018). Hybrid Investigation on the Hydraulic Performance of a New Trapezoidal Fishway. Daniel Bung, Blake Tullis, 7th IAHR International Symposium on Hydraulic Structures, Aachen, Germany, 15-18 May. doi: 10.15142/T3S06R (978-0-692-13277-7).

7th International Symposium on Hydraulic Structures Aachen, Germany, 15-18 May 2018
ISBN: 978-0-692-13277-7 DOI: 10.15142/T3S06R

Hybrid Investigation on the Hydraulic Performance of a New Trapezoidal Fishway

D.B. Bung[1], D. Valero[1] & G. Hermens[2]
[1]*Hydraulic Engineering Section, Aachen University of Applied Sciences, Aachen, Germany*
[2]*Floecksmühle GmbH, Aachen, Germany*
E-mail: bung@fh-aachen.de

Abstract: *The current study presents a new type of vertical slot fishway. The main difference of this trapezoidal fishway compared to the standard design of a vertical slot fishway remains in the separation of the pools into two zones: the migration corridor and the energy dissipation zone. The structure is first investigated in a physical model to optimize the training walls and slot geometry in order to avoid recirculation of the flow. Velocity and flow depth data from experimental flow measurements is later compared to the three-dimensional numerical model which provides a deeper insight into the flow field. The proposed design is found to avoid large vortices within the migration corridor. Moreover, uniform flow conditions are also found within the energy dissipation zone, thus providing an alternative corridor for fish passage.*

Keywords: *Fish passage, physical modeling, numerical modeling, CFD, vertical slot fishway.*

1. Introduction

Many natural water bodies have been heavily modified in the last century. In Europe, the Water Framework Directive (EU-WFD 2000) targets for a good status of all European water bodies by the year 2027. River morphology is a key parameter. In this regard, river continuity must not be disturbed by anthropogenic activities and migration of aquatic organisms must be allowed. At weirs and dams which cannot be removed, fishways serve as ecological bridges to help restore river connectivity. These fishways can be built in technical or nature-like manners and have been the subject of intensive research in the past (Katopodis and Williams 2012). Some studies report that nature-like and technical pool-slot facilities are most efficient (Bunt et al. 2012; Noonan et al. 2012).

As for technical fishways, the vertical slot fishway – being developed in the Unites States in the second half of the 20th century (DVWK 2002; Clay 1961; Rajaratnam et al. 1986.; Wu et al. 1999; Puertas et al. 2004) – is the most popular. This type of fishway typically consists of a rectangular cross-section. The total drop height between the upstream and downstream water level is continuously overcome by several smaller drops of constant height Δh between adjacent pools. The cross-walls separating two pools are notched by vertical slots extending over the full wall height. All slots are located at one side of the structure in order to create pools with areas of lower flow velocities on the opposite side. Baffle blocks are commonly installed downstream of the slots to deflect the water into the pools where most of the kinetic energy is dissipated, thus avoiding high-velocity short-circuit flow through the slots. Due to this flow deflection, some recirculation takes place in the pools which may disorient fish. Moreover, fish migration has to take place through this high-turbulence flow area, which may exceed the swimming capabilities of various migratory fish species (e.g., salmonids) and aquatic life (eels, crayfish, etc.) with their respective life stages considered during design.

This study presents a new design of a vertical slot fishway – i.e. the trapezoidal fishway – which aims to provide low-turbulent and uniform flow in the migration corridor. A hybrid modeling approach is applied to investigate the flow field. The application of three-dimensional numerical models in fishway design has become popular in the recent years (Quaranta et al. 2017) and provides a better understanding of the complex flow in the pools (Fuentes-Pérez et al. 2018). All tests are performed under consideration of the barbel zone, where Cyprinidae, such as barbel, dominate but also larger fish like brown trout and salmon can be found. Hydraulic and geometric design requirements for classical vertical slot fishways, according to the German standard DWA (2014), are assumed.

2. Design Parameters for Vertical Slot Fishways

Pool and slot dimensions depend on the size of adult fish of the expected species. For the barbel zone considered in this study, dimensions of selected fish according to DWA (2014) can be found in Table 1:

Table 1. Fish dimensions in barbel zone.

Species	Length l_{Fish} [m]	Width w_{Fish} [m]	Height h_{Fish} [m]
Barbel	0.7	0.08	0.13
Brown trout	0.8	0.09	0.17
Salmon	1.0	0.10	0.17

Significant fishway dimensions – namely the pool length, pool width, and slot width – depend on the largest expected fish species. Their definitions in a vertical slot fishway are illustrated in Fig. 1. In order to allow fish to perform complex swim maneuvers, such as acceleration, deceleration, and change in direction, the pool length l_{Pool} should have a minimum length of three times the length of the largest adult fish species:

$$l_{Pool} \geq 3 \times l_{Fish,max} \tag{1}$$

The width of a pooled fishway should be

$$0.5 \times l_{Pool} \leq w_{Pool} \leq 0.67 \times l_{Pool} \tag{2}$$

to attain low-turbulence flow and guarantee sufficient volumetric power dissipation while a minimum slot width of

$$s \geq 3 \times w_{Fish} \tag{3}$$

should be considered to ensure a safe passage of fish. It should be noted that, as a rule of thumb, a more conservative pool width of

$$w_{Pool} = 0.75 \times l_{Pool} \tag{4}$$

is often regarded for slot fishways to ensure sufficient energy dissipation. However, this value is not considered in this study.

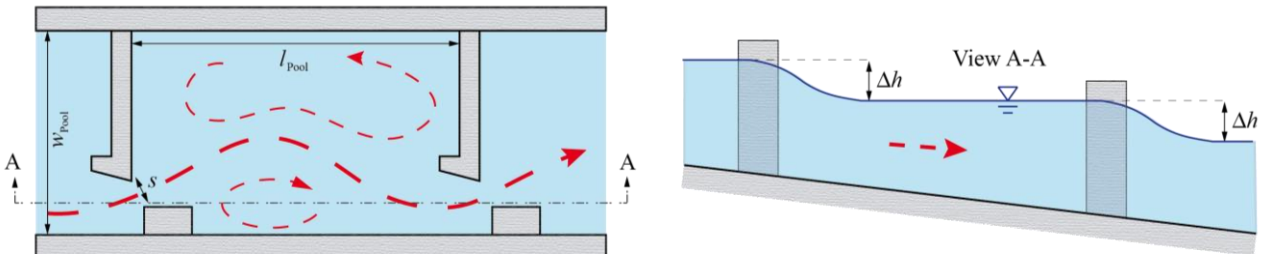

Figure 1. Schematic sketch of a classical vertical slot fishway and significant dimensions, left: top view, right: longitudinal section (flow from left to right, note the recirculation zones in the pool).

With these requirements, a vertical slot fishway in the considered barbel zone must have the following minimum dimensions according to DWA (2014):

Table 2. Pool dimensions in the considered barbel zone.

Species	Length l_{Pool} [m]	Width w_{Pool} [m]	Slot width s [m]
Barbel	2.1	1.05	0.25
Brown trout	2.4	1.20	0.27
Salmon	3.0	1.50	0.30

Particularly for long fishways, it is most important to keep a minimum flow depth and not exceed a maximum permissible flow velocity. While migration close to the free surface may attract natural enemies, migration near the bed may cause injuries to the fish. A sufficient water depth is thus necessary to allow the fish swimming within the water column to have adequate distance from both boundaries. With the height of adult fish given in Table 1, the minimum water depths according to DWA (2014) may be estimated as:

$$h_{min} = 2.5 \times h_{Fish} \tag{5}$$

with consideration of the largest fish species. Downstream of the slots, the required water depth may be assumed as $2 \times h_{Fish}$ as fish generally accept such shallow water conditions for very short distances.

As for the flow velocities, the swimming capacity of the weakest species needs to be regarded. Fastest swimming speeds can only be maintained for some seconds with the consequence that the highest flow velocities have to be limited to the slot area. With increasing the total length of the fishway, the maximum velocity in each pool needs to be reduced in order to guarantee that the fish can pass the entire structure and to avoid exhaustion or that the fish is drifted with the flow. For the barbel zone, maximum permissible local flow velocities are $1.6 \leq v_{max} \leq 1.8$ m/s, depending on the total drop height. It must be noted that these values should be reduced by a design factor to account for the uncertainty of the underlying data. However, in this study these characteristic values are considered. Additionally, a minimum flow velocity (i.e. the rheoactive speed) is needed to attract fish, make it align with the flow and swim against the current. For the species considered herein, v_{min} should be 0.3 m/s (DWA 2014).

The energy dissipation factor *EDF* as a measure of turbulence within a pool and can be estimated by

$$EDF = \rho_w \times g \times Q \times \Delta h/V \tag{6}$$

with ρ_w the density of water, Q the discharge, and V the water volume in the pool. For the considered barbel zone, p_D should be below 150 W/m^3. All aforementioned hydraulic design values are summarized again in Table 3.

Table 3. Required hydraulic conditions for the considered barbel zone (* values in brackets refer to the slot zone).

Species	Water depth h_{min}* [m]	Velocity v_{min} [m/s]	Velocity v_{max} [m/s]	Energy dissipation *EDF* [W/m^3]
Barbel	0.33 (0.26)	0.30	1.60 - 1.80	150
Brown trout	0.42 (0.33)			
Salmon	0.42 (0.34)			

2.1. Trapezoidal Fishway

A drawback of the classical vertical slot fishway (and other fishways as well) is given by a combined energy dissipation and migration zone which results in relatively high flow velocities in the migration corridor. Moreover, recirculations, as illustrated in Fig. 1, may disorient fish.

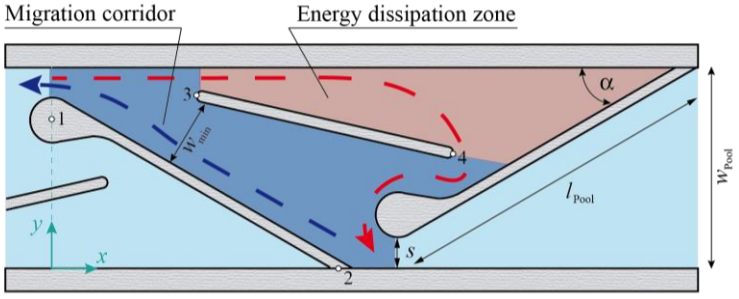

Figure 2. Schematic sketch of the proposed trapezoidal fishway and main dimensions, energy dissipation zone shaded in red color, migration corridor shaded in blue color (flow from left to right).

An improvement of fish passage facilities may be the separation of a migration corridor and an energy dissipation zone. The flow velocity in the migration corridor may be partly higher but should not be lower than the rheoactive speed. Moreover, no large eddies are desirable. No special demands for hydraulic conditions, however, are made on the energy dissipation zone. Flow recirculation may be avoided by installing a training wall between both zones. A potential structure to fulfill these requirements may be a fishway as illustrated in Fig. 2. This fishway is divided into pools by diagonally orientated walls with single slots alternately on the left and the right sidewall. The basins may thus have a triangular or trapezoidal shape.

Special care needs to be taken regarding the slot design to assure uniform flow conditions at the pool inlet. It must be noted that for narrow migration corridors as the one in Fig. 2, a minimum width w_{min} of $6w_{Fish}$ should be given according to DWA (2014).

3. Modeling Description

3.1. General Remarks

The current study makes use of a hybrid modeling approach. A physical model is built to investigate flow fields and to optimize flow conditions. The aim of this optimization is to (i) separate the migration corridor from the energy dissipation zone, (ii) to ensure that no reverse flow occurs in the migration corridor, and (iii) to avoid flow contractions in the slot and thus ensure uniform flow at the pool inlets. It must be noted that multiple setups have been investigated experimentally in this study but are not further described subsequently. Instead, only the best solution found in the laboratory (Case 4 in Fig. 3e) is studied in more detail, employing numerical simulations. However, four selected additional configurations are shown in Fig. 3. The following flow characteristics were found in the experiments:

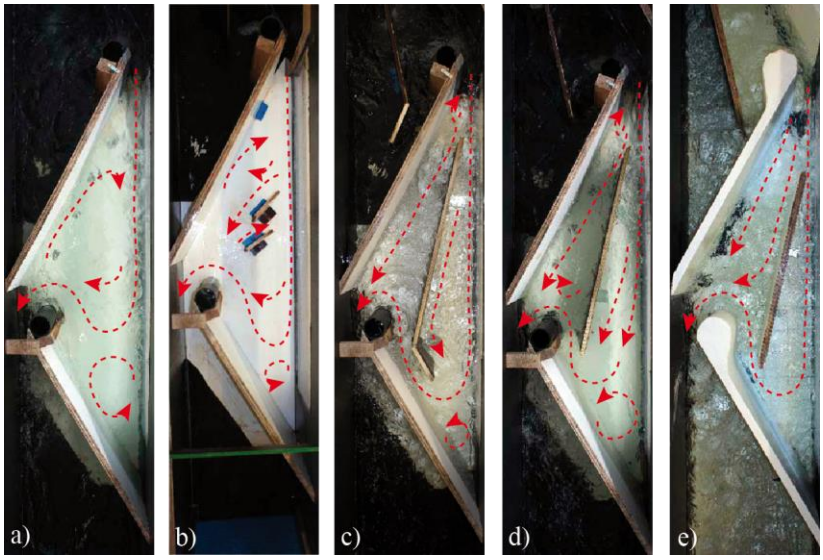

Figure 3. Top view photos of selected different configurations modeled in the laboratory and resulting flow fields, (a) reference case 0 (without separation of migration and energy dissipation zone), (b) case 1 with separation by means of two deflectors, (c) case 2 with a long, bent training wall, (d) case 3 with separation by a training wall without optimization of the slot geometry, (e) case 4 with optimized positioning of the training wall and large roundings at slot inlets (flow from top to bottom).

Case 0: This reference case does not fulfill the requested separation of migration and energy dissipation zone but provides some insight into the flow field in a trapezoidal pool without any training walls. A well-defined migration corridor can be found. However, due to strong recirculation this configuration is not suitable for prototype design.

Case 1: The single vertical deflectors are installed to successfully separate the migration and energy dissipation zone. However, large vortices are found around these deflectors, which may again disorient fish.

Case 2: A long, bent training wall is installed which separates the migration corridor from the energy dissipation zone. It is found that this geometry avoids large-scale vortices and provides a well-defined migration corridor with adequate flow velocities. However, it is tested in the next case if the complex, bent geometry can be simplified.

Case 3: Satisfactory flow conditions are found along the migration corridor being separated from the energy dissipation zone by a long training wall. Additionally, relatively low flow velocities are found in the energy dissipation zone, thus providing a second corridor of sufficient width for disoriented fish.

Case 4: This is the optimum case based on case 3, but with larger rounding at the slot inlet to avoid flow separation and undesired flow recirculation in the migration corridor. Moreover, the training wall position is slightly adjusted to increase the width of the migration corridor.

While in the physical model, only local measurements of flow depths and velocities can be conducted, the numerical model provides detailed information on the entire flow field inside the pools. Experimental data is used to calibrate and validate the numerical model.

3.2. Experimental Setup

The physical model was constructed in the hydraulic laboratory of FH Aachen with scale 1:3.9 and a total length of 5.0 m. It consists of an inflow area, two pools and an outflow area (see Fig. 4). All measurements are conducted in the second pool, which is equipped with a window to observe the flow patterns.

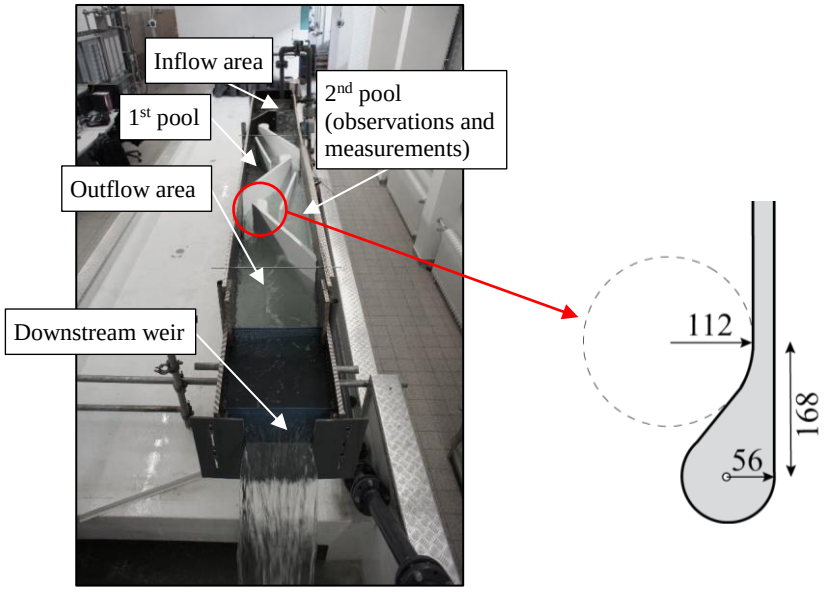

Figure 4. Physical model (here: case 4) at FH Aachen, left: overview (flow from top to bottom), right: detail sketch of the rounding at slots (in mm).

With salmon as the largest considered fish in this study, the slot width is kept constant with s = 0.076 m. The pool length l_{Pool} is > 0.77 m in all setups, depending on the slot geometry, and α is 33° for all tests. The pool (and flume) width w_{Pool} is 0.5 m and the bottom slope is 5 %.

Given the model length scale of 1:3.9, the velocity scale becomes 1:1.97 according to Froude's similitude and following critical values of design parameters in Table 4 have to be considered:

Table 4. Required hydraulic conditions for the considered barbel zone in model scale (* value in brackets refers to the slot zone).

Water depth h_{min}* [m]	Velocity v_{min} [m/s]	Velocity v_{max} [m/s]	Energy dissipation *EDF* [W/m^3]
0.108 (0.087)	0.15	0.81 – 0.91	76

All walls are 28 mm thick. With respect to the coordinate system and the points 1 to 4, as marked in Fig. 2, the final geometry in case 4 is defined as follows:

Table 5. Final geometry of the trapezoidal fishway tested in case 4.

Point	x [m]	y [m]
1	0.000	0.369
2	0.838	0.000
3	0.379	0.427
4	0.990	0.286

The model is part of a closed water circuit. Water discharge is regulated with a butterfly valve and controlled with an inductive flow meter. The water is pumped into an upstream head tank with a capacity of 125, l being installed below the flume before being smoothly conveyed into the channel. A perforated steel sheet is used to ensure uniform inflow conditions at the inlet. A rectangular, sharp-crested weir of 30 cm width is used to set the downstream flow depth and to validate the flow rate. Applying the Rehbock weir equation, a maximum difference of 5 % was found compared to the flow meter.

Flow velocities are measured with an anemometer with a measuring range of 0.05 to 5.00 m/s (Schiltknecht MiniWater 6 Micro). This anemometer is connected to a universal amplifier (HBM MX 840a), while the sample rate is set to 50 Hz, the true response time of the sensor is larger due to the inertia of the helix. The probe has a diameter of only 11 mm and an accuracy of ± 3.5 % according to supplier specifications. The probe is manually positioned and rotated until the maximum velocity magnitude is reached. All measurements are taken at 8.5 cm below the water surface and averaged over 60 s.

Flow depths are measured by means of an ultrasonic sensor for 60 s with a sample rate of 50 Hz. The sensor (microsonic mic+130/IU/TC) is again connected to the HBM amplifier. Its measuring range is 200 to 2,000 mm with an accuracy of 1 %. The flow rate and downstream water level are adjusted until uniform flow (identical water levels at similar locations in pool 1 and pool 2 is obtained. For the case presented (case 4), the model is operated with a downstream water level of 18.0 cm and a discharge of 12.3 l/s.

3.3. Numerical Model

The 3D numerical model is set up using the commercial code FLOW-3D®, using a Finite Volume Method (Versteeg and Malalasekera 2007). The RNG k-ε turbulence model (Yakhot and Orszag 1986; Yakhot et al. 1992) is employed to solve the RANS equations on a mesh with three mesh blocks. Spatial discretization is refined around the second pool (mesh block 2) in the section $0 \leq x \leq 1.62$ m, allowing study of the mesh dependency (with $x = 0$ at the upstream slot as defined in Fig. 2, while a coarser mesh is used for the inflow area and the first pool (mesh block 1) as well as for the outflow area (mesh block 3). Meshes 1 and 3 serve as "buffer" meshes to allow realistic boundary conditions at the inlet and outlet of mesh 2, which discretizes the main region of interest. The model is set up in a 1-fluid-approach (Prosperetti and Tryggvason 2007), and the Volume of Fluid (VOF) method is applied for the dynamic determination of the free-surface (Hirt and Nichols 1981). The downstream boundary condition is specified as a hydrostatic pressure while the upstream boundary condition is set as a specified flow rate. Lateral boundary conditions are set to symmetry (frictionless with null normal flow) as the wall friction is assumed to be negligible. The model is initially filled with a water body of 20 cm height. The flume geometry is modeled horizontally, but gravity is set to 0.49 m/s^2 in the flow direction in order to account for the bottom slope of 5 %. All simulations are run for 30 s. Numerical data is finally time-averaged over the last 3 s (which were found to be quasi-steady) for further analysis.

For analysis of the mesh dependency, cubic cells with five different cell sizes in mesh block 2 are considered, namely Δx = 15 mm, 10 mm, 7.5 mm, 5 mm, and 3.8 mm. The cell size in the coarse mesh blocks 1 and 3 is constant with Δx = 15 mm. This value has been chosen to preserve a cell size ratio larger than 4 for all configurations. The convergence is subsequently checked for water depths and depth-averaged velocities. Fig. 5 presents this data for all mesh resolutions $1/\Delta x$ for three selected locations. The first location (x = 0.02 m, y = 0.46 m) is located at the center of the upstream slot, the second location (x = 0.65 m, y = 0.20 m) refers to the migration corridor, while the third location represents the energy dissipation zone (x = 0.90 m, y = 0.40 m). It is found that the results converge well for the flow depths, but some detrended oscillations are still found for the velocity magnitudes at the slot area and the energy dissipation zone. While this result may have been expected for the high-turbulent slot area, the lower convergence in the energy dissipation zone may be explained by the change of flow direction at this location (as will

be shown in the flow field in Fig. 8). However, the lower convergence for velocity data is a known issue for similar types of fields as it was also shown by Fuentes-Pérez et al. (2018) for vertical slot fishways.

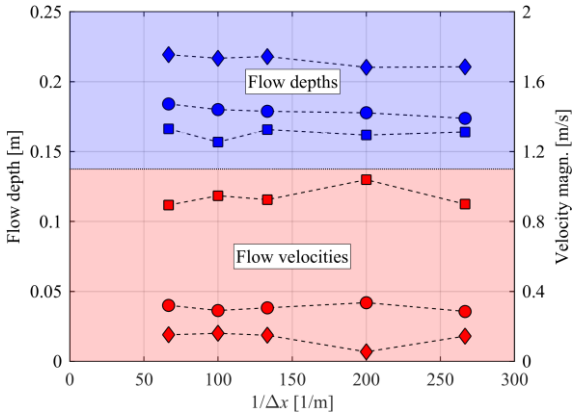

Figure 5. Convergence of flow depths and velocity magnitude at three selected locations for five cell sizes (Δx = 15 mm, 10 mm, 7.5 mm, 5 mm, and 3.8 mm); in the slot (x = 0.02 m, y = 0.46 m, ■/■), migration corridor (x = 0.65 m, y = 0.20 m, ●/●) and energy dissipation zone (x = 0.90 m, y = 0.40 m, ♦/♦), red markers for flow velocities, blue markers for flow depths.

Flow depths and flow velocities are measured at several locations within the second pool as described above. This data is used for calibration and validation of the model. The results from the numerical simulations are compared to this laboratory data in Fig. 6. In order to check the mesh convergence for more data points, numerical results are displayed for all studied cell sizes. It is found that the numerical data generally tends to converge towards the perfect line, with flow depths comparing better to the laboratory data, as scattering is lower than for the flow velocities. Nonetheless, some data points deviate significantly from the lab data. A deeper analysis showed that these points are located directly downstream of the slot where a steep water surface is found due to the acceleration of the flow. It may be assumed that the employed ultrasonic sensors provide less accurate data in such type of flow (Zhang et al. 2018). Flow velocities are found to generally scatter more. Here, it must be noted that the employed 1D velocity meter may be assumed to be of low accuracy as it is too slow to detect high-turbulent velocity fluctuations. Some additional uncertainty arises from the three-dimensional type of flow in the fishway. Note that the locations of all laboratory measurements are shown in Fig. 7 and 8. Despite these deviations, numerical data compares well to the laboratory data, and hence the numerical results from the finest mesh are considered for further analysis.

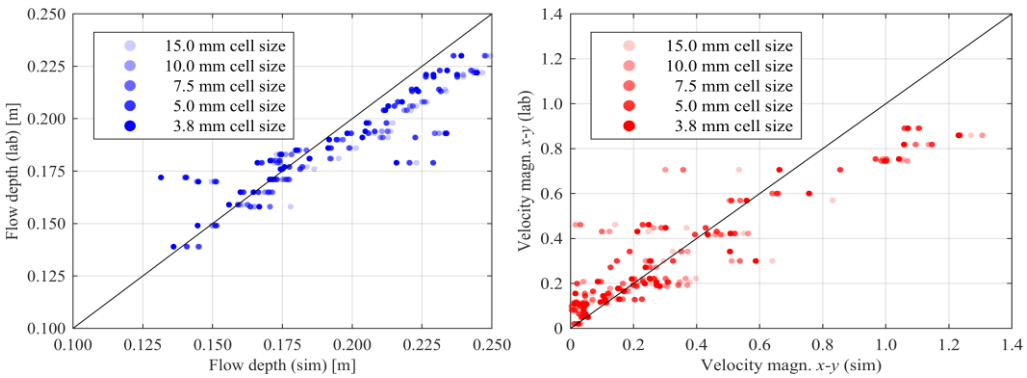

Figure 6. Convergence of flow depth and velocity magnitude in x-y plane for different cell sizes (15 mm, 10 mm, 7.5 mm, 5 mm, and 3.8 mm), numerical data (sim) comparison to experimental data (lab); left: flow depth, right: flow velocity.

4. Results

4.1. Flow Depths

Flow depths from the numerical simulation are illustrated in Fig. 7. It is found that similar water levels are found on both sides of the training wall separating the migration corridor from the energy dissipation zone. The highest water level sets in at the end of the latter. However, given the bottom slope of 5 %, the water surface is roughly horizontal.

A steeper water surface gradient is found in the migration corridor, but the minimum required water levels are given at every location. Lowest water levels are in the range of about 13 cm near the slots (see also Fig. 6 left).

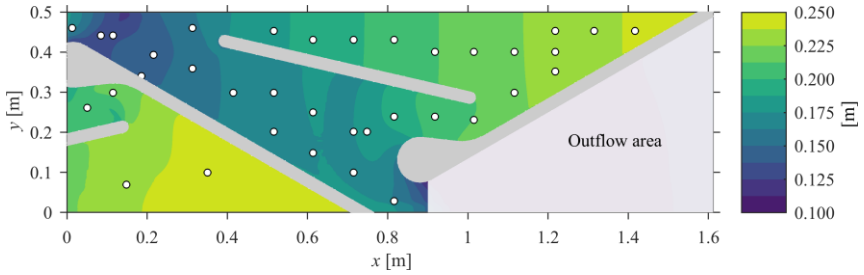

Figure 7. Water depth in pool 2 from the numerical simulation with 3.8 mm cell size, markers indicate the locations of measuring points in the laboratory (flow from left to right).

4.2. Flow Velocities and Flow Field

Fig. 7 shows that the flow field from the numerical model compares well to the lab observations (see Fig. 3e). The arrangement of the training wall successfully suppresses the generation of large vortexes. Instead, the flow is straight and uniform in both zones. While at the downstream end of the energy dissipation zone, velocities below the critical value are predominant, the flow velocities along the migration corridor are mostly on the range of 0.3 m/s in model scale (0.59 m/s in prototype scale). This velocity is sufficiently high to activate the positive rheotaxis and lead fish to face into the current and continue the upstream migration. It must be pointed out that the maximum velocity condition of v_{max} = 0.91 m/s in model scale (1.80 m/s in prototype scale) is not met in a small area downstream of the slot (at $x \approx 0.1$ m). The corresponding cross-section is highlighted by a white dashed line in Fig. 8.

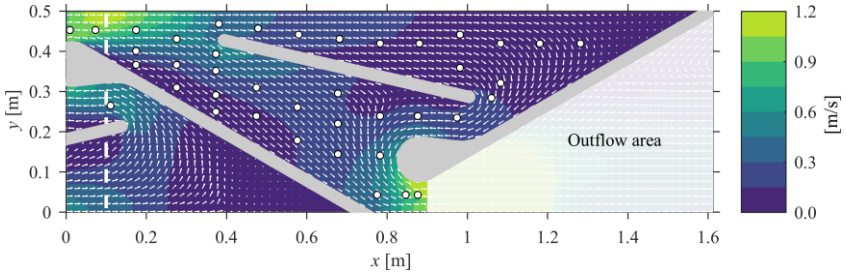

Figure 8. Depth-averaged velocity magnitude in pool 2 from the numerical simulation with 3.8 mm cell size, markers indicate the locations of measuring points in the laboratory (flow from left to right), white dashed line indicates the location of cross-section shown in Fig. 9, velocity vectors are normalized (only every 5th vector is displayed).

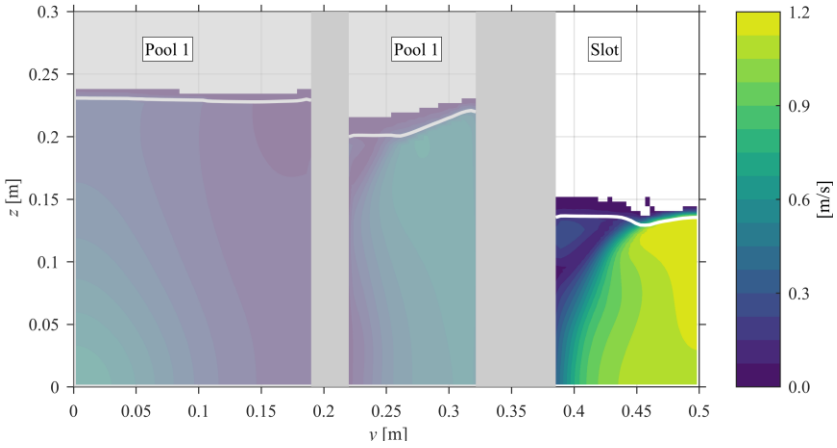

Figure 9. Distribution of the velocity magnitude at x = 0.1 m downstream of the slot, areas corresponding to pool 1 are shadowed to highlight the slot area, white line indicates the free-surface location according to the VOF method.

The vena contracta is, however, limited to a small area near the wall. The velocity magnitude distribution in the *y*-*z*-plane at $x = 0.1$ m is presented in Fig. 9. It can be observed that the flow velocity limit is exceeded in approximately half of the cross-section while a potential migration corridor still exists near the training wall. Adam and Lehmann (2011) describe detailed laboratory tests at vertical slot fishways in prototype scale observing the migration behavior of different fish species. The authors state that all species, adult and juvenile fish, could pass the vena contracta or, for increasing flow velocities, tended to swim around it. They conclude that the flow velocity within the slots, and not the maximum value in the vena contracta, is crucial for fish migration. It may thus be assumed that the efficiency of the herein studied trapezoidal fishway is not affected by this local velocity exceedance. The mean velocity magnitude in the slot area shown in Fig. 9 ($0.385 \leq y \leq 0.5$) is found to be 0.78 m/s (1.54 m/s in prototype scale), while the averaged velocity in the slot is 0.91 m/s (1.80 m/s in prototype scale) and thus matches the critical value.

Fig. 10 illustrates the streamlines in both the energy dissipation zone and the migration corridor, originating from the slot section with 7.5 mm spacing to underline the uniformity of the flow. The vortex-free flow which was already observed in the depth-averaged flow field in Fig. 8 is also found for the fully three-dimensional flow field.

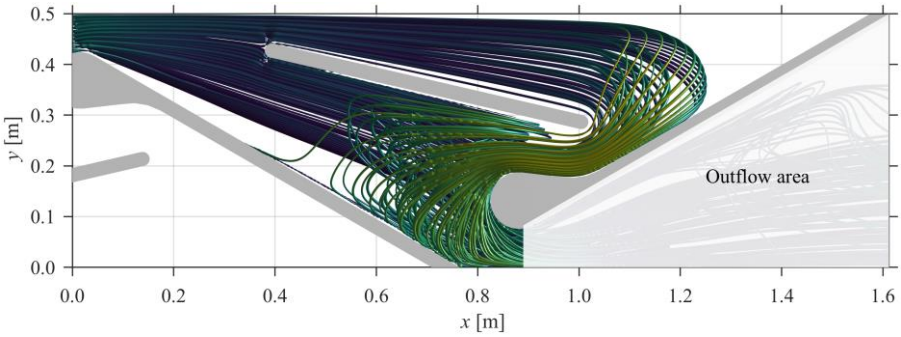

Figure 10. Streamlines in pool 2 from the numerical simulation with 3.8 mm cell size, streamlines originating from the slot with 7.5 mm spacing, note the uniform flow in the migration corridor as well as in the energy dissipation zone (flow from left to right).

4.3. Energy Dissipation

A volumetric flow rate of 4.1 l/s enters the energy dissipation zone while 8.2 l/s are discharged through the migration corridor. The EDF as an indirect measure of turbulence is estimated by Eq. (6), assuming uniform flow conditions ($\Delta h = 0.05 l_{Pool}$) and the water volumes in each zone as considered in Fig. 2. While the energy dissipation zone shows an energy dissipation factor of 47 W/m^3, EDF in the migration corridor is 93 W/m^3 and thus higher than the maximum value of 76 W/m^3. However, it is a known issue for general vertical slot fishways that the pool width, which directly affects the water volume and thus EDF, should be designed larger than the value resulting from Eq. (2). It may be assumed that the hydraulic performance of the trapezoidal fishway in terms of its energy dissipation potential is comparable to the one obtained in the vertical slot fishways. A wider pool, however, could not be tested in the laboratory due to a fixed flume width.

5. Conclusions

A new design of a vertical slot fishway is proposed in this paper and its hydraulic performance is tested using a hybrid modeling approach. Physical model data is used for optimization of the general design and for validation of the numerical model. The main goal of the new trapezoidal fishway is to separate the migration corridor from the energy dissipation zone to ensure a low-turbulence, vortex-free area improving the upstream migration performance. It was shown that with the final design, uniform flow conditions are established in both zones, thus also allowing the fish migration through in the energy dissipation zone. The minimum flow velocity, which is needed to activate the positive rheotaxis, is obtained in the migration corridor only while the downstream end of the energy dissipation zone shows even lower velocities. Maximum velocities are exceeded downstream of the slots as it is often found in vertical slot fishways. It was found that the energy dissipation factor is higher in the migration corridor and exceeds the critical value. A wider design of the structure may help to improve the energy dissipation performance.

The study so far focused on the hydraulics only. In order to evaluate the fish migration performance, prototype scale tests with fish are required.

6. Acknowledgements

The experimental data has been gathered in the framework of a Master thesis at FH Aachen by M.Eng. Jeff Haag. The concept of the trapezoidal fishway has been developed by Dipl.-Ing. Ulrich Dumont (Floecksmühle GmbH, †) who was also external advisor of the student.

7. References

Adam, B., and Lehmann, B. (2011). Ethohydraulik: Grundlagen, Methoden und Erkenntnisse. Springer, Berlin (in German).

Bunt, C.M., Castro-Santos, T., and Haro, A. (2012). "Performance of fish passage structures at upstream barriers to migration." *River Res. Applic.*, 28(4), 457-478.

Clay, C.H. (1961). Design of fishways and other fish facilities, Dept. of Fisheries of Canada, Ottawa.

DVWK (2002). Fish passes—Design, dimensions and monitoring, Food and Agriculture Organization of the United Nations / Deutscher Verband für Wasserwirtschaft und Kulturbau e.V. (DVWK), Rome.

DWA (2014). Fischaufstiegsanlagen und fischpassierbare Bauwerke—Gestaltung, Bemessung, Qualitätssicherung, German Association for Water, Wastewater and Waste (DWA), Guideline M 509, Hennef (in German).

EU-WFD (2000). Directive 2000/60/EC of the European Parliament and of the Council establishing a framework for the Community action in the field of water policy (EU Water Framework Directive).

Fuentes-Perez, J.F., Silva, A.T., Tuhtan, J.A., García-Vega, A., Carbonell-Baeza, R., Musall, M., and Kruusmaa, M. (2018). "3D modelling of non-uniform and turbulent flow in vertical slot fishways." *Environ. Model. Softw.*, 99, 156-169.

Hirt C.W., and Nichols, B.D. (1981). "Volume of fluid (VOF) method for the dynamics of free boundaries." *J. Comput. Phys.*, 39(1), 201-225.

Katopodis, C., and Williams, J.G. (2012). "The development of fish passage research in a historical context." *Ecol. Eng.*, 48, 8-18.

Noonan, M.J., Grant, J.W.A., and Jackson, C.D. (2012). "A quantitative assessment of fish passage efficiency." *Fish Fish*, 13(4), 450-464.

Prosperetti, A., and Tryggvason, G. (2007). Computational methods for multiphase flow. Cambridge Press, Cambridge.

Puertas, J., Pena, L., and Teijeiro, T. (2004). "Experimental approach to the hydraulics of vertical slot fishways." *J. Hydr. Eng.*, 130(1), 10-23.

Quaranta, E., Katopodis, C., Revelli, R., and Comoglio, C. (2017). "Turbulent flow field comparison and related suitability for fish passage of a standard and a simplified low-gradient vertical slot fishway." *River Res Applic*., 33(8), 1295-1305.

Rajaratnam, N., Van der Vinne, G., and Katopodis, C. (1986). "Hydraulics of vertical slot fishways." *J. Hydr. Eng.*, 112(10), 909-927.

Versteeg, H.K., and Malalasekera W. (2007). An introduction to computational fluid dynamics: the finite volume method. Pearson Prentice Hall, Harlow.

Wu, S., Rajaratnam, N., and Katopodis, C. (1999). "Structure of flow in vertical slot fishway." *J. Hydr. Eng.*, 125(4), 351-360.

Yakhot, V., and Orszag, S.A. (1986). "Renormalization group analysis of turbulence. I. Basic theory." *J. Sci. Comput.* 1(1), 3-51.

Yakhot, V., Orszag, S.A., Thangam, S., Gatski, T.B., and Speziale, C.G. (1992). "Development of turbulence models for shear flows by a double expansion technique." Phys. Fluids A, 4(7), 1510-1520.

Zhang, G., Valero, D., Bung, D.B., and Chanson, H. (2018). "On the estimation of free-surface turbulence using ultrasonic sensors." Flow Meas. Instrum, in review.